nature biomedical engineering

Article

https://doi.org/10.1038/s41551-023-01128-9

Screening oral drugs for their interactions with the intestinal transportome via porcine tissue explants and machine learning

Received: 9 November 2020

Accepted: 1 October 2023

Published online: 20 February 2024

Check for updates

Yunhua Shi[1,2,7], Daniel Reker[1,2,3,7], James D. Byrne[1,2,4,5], Ameya R. Kirtane[1,2], Kaitlyn Hess[1], Zhuyi Wang[1], Natsuda Navamajiti[1,6], Cameron C. Young[2], Zachary Fralish[3], Zilu Zhang[3], Aaron Lopes[1], Vance Soares[1], Jacob Wainer[1], Thomas von Erlach[1], Lei Miao[1], Robert Langer[1] & Giovanni Traverso[1,2,4] ✉

In vitro systems that accurately model in vivo conditions in the gastrointestinal tract may aid the development of oral drugs with greater bioavailability. Here we show that the interaction profiles between drugs and intestinal drug transporters can be obtained by modulating transporter expression in intact porcine tissue explants via the ultrasound-mediated delivery of small interfering RNAs and that the interaction profiles can be classified via a random forest model trained on the drug–transporter relationships. For 24 drugs with well-characterized drug–transporter interactions, the model achieved 100% concordance. For 28 clinical drugs and 22 investigational drugs, the model identified 58 unknown drug–transporter interactions, 7 of which (out of 8 tested) corresponded to drug-pharmacokinetic measurements in mice. We also validated the model's predictions for interactions between doxycycline and four drugs (warfarin, tacrolimus, digoxin and levetiracetam) through an ex vivo perfusion assay and the analysis of pharmacologic data from patients. Screening drugs for their interactions with the intestinal transportome via tissue explants and machine learning may help to expedite drug development and the evaluation of drug safety.

Drug transporters are membrane proteins that have been recognized as major determinants of the pharmacokinetics, biodistribution and efficacy of drugs[1–3]. A major focus in drug discovery and development is to understand the transportome[4] and the interaction between drugs and their transporters[5], specifically in the context of their role in determining intestinal absorption of orally administered medications. Current systems used to study transporter–drug interactions include engineered cell monolayers and vesicular assays[6–9]. Such simplified models often fail to accurately capture the complex and dynamic cellular context and do not capture differences in transporter-expression levels or the cellular heterogeneity of native tissues[10–14]. Knockout and humanized mice can act as models with higher physiological relevance, but low throughput and high cost limit their broader application[7,15]. Importantly, none of these approaches enable the controlled and fine-tuned manipulation of individual expression levels to study the complex interplay between transporters[16] and their joint impact on the

[1]Koch Institute for Integrative Cancer Research, Massachusetts Institute of Technology, Cambridge, MA, USA. [2]Division of Gastroenterology, Department of Medicine, Brigham and Women's Hospital, Harvard Medical School, Boston, MA, USA. [3]Department of Biomedical Engineering, Duke University, Durham, NC, USA. [4]Department of Mechanical Engineering, Massachusetts Institute of Technology, Cambridge, MA, USA. [5]Department of Radiation Oncology, University of Iowa, Iowa City, IA, USA. [6]Department of Biomedical Engineering, Chulalongkorn University, Bangkok, Thailand. [7]These authors contributed equally: Yunhua Shi, Daniel Reker. ✉e-mail: cgt20@mit.edu

https://doi.org/10.1038/s41551-023-01128-9

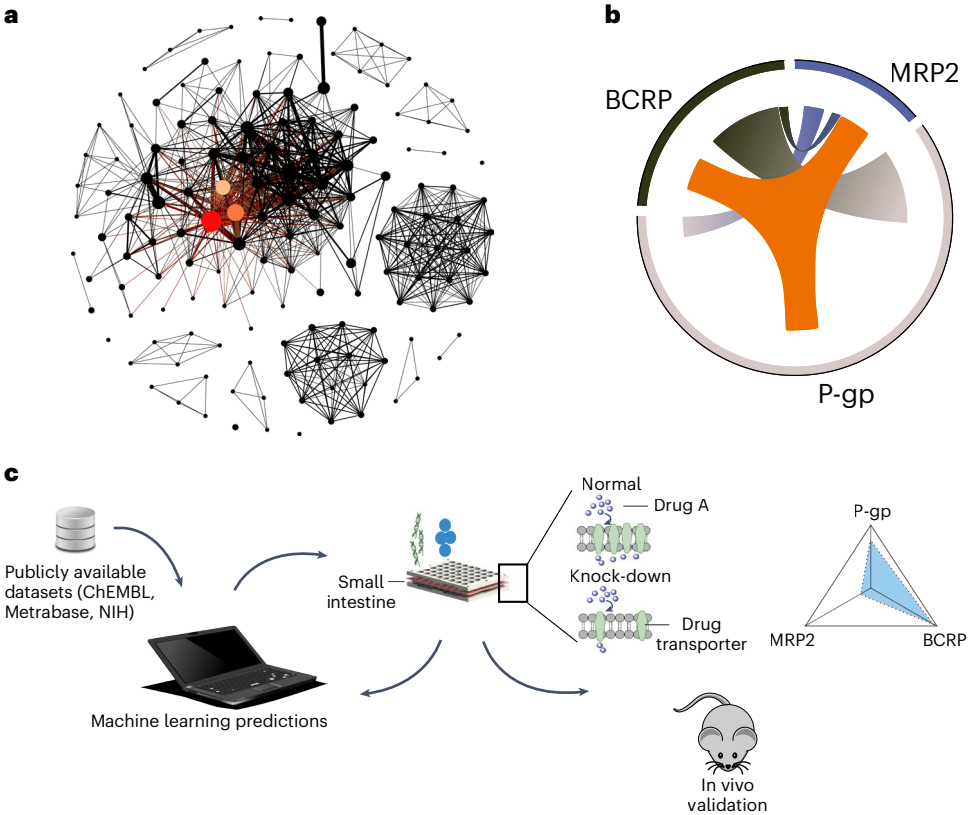

Fig. 1 | Transportome interactions and schematic of the closed-loop pipeline to predict and validate drug transport profiles. a, Relying on DrugBank data, we estimated that the 149 currently known drug transporters form a complex interaction network with a total of 1,891 known transportome interactions, that is, pairs of drug transporters with at least one shared substrate. The transportome interactions span a complex and disjointed network, with multiple classes of transporters sharing multiple substrates while also not sharing substrates with other drug transporters. The three transporters with the largest number of known substrates are highlighted in colour: red, P-gp; orange, BCRP; yellow, MRP2. **b**, Known interactions between the three drug transporters P-gp, BCRP and MRP2. Circle fraction is indicative of relative number of substrates per transporter, corresponding to 186, 70 and 43 substrates annotated for P-gp, BCRP and MRP2 in DrugBank 5.0, respectively. Shared substrates are connected through proportional surfaces. P-gp and BCRP share 48 substrates, BCRP and MRP2 share 19, and P-gp and MRP2 share 24. In addition, 15 substrates are annotated to be shared by all three transporters (orange). **c**, We have curated a large database of drug transport interactions with 4,554 annotations for 2,261 small-molecule drugs and screening compounds from three individual data sources (DrugBank, Metrabase, NCI-60) and additional, machine-learning-guided literature search. We utilized these data to build a state-of-the-art random forest machine-learning model. The physical and chemical properties of a new potential drug are incorporated into a random forest-based machine-learning algorithm to generate predictions of the potential substrate relationship with various drug transporters. On the basis of the prediction report, a series of siRNA-induced drug transporter knock-downs are performed on an ex vivo porcine small-intestine tissue-based screening system. These ex vivo data were fed back into the machine-learning algorithm to further modify the database and improve the predictive performance. Identified substrate relationships were subsequently validated in vivo.

bioavailability of medications. In silico models are becoming increasingly accurate and are an important tool to streamline the experimental identification of transporter–drug interactions[17–20], but there is a lack of explicit integration of computational tools and experimental systems[21]. Such set-ups would enable feedback-driven machine learning to continuously improve predictions and models[22], which is of particular relevance for the prediction of transporter–drug interactions, given the variance and heterogeneity of available data that continue to be acquired through simplified and distinct model systems without standardized protocols, controls or readouts[21,23,24].

Our system uses intact, ex vivo porcine tissue to model intestinal drug transport in a physiologically relevant context with similar cellular structure and protein expression to what would be found in humans[25–28]. Several studies have shown the application of porcine intestinal tissue as a model for human drug-transport studies[29–34]. Therefore, we believe that this tissue-based system provides a compromise between the simplicity of cell-based assays and the physiological relevance of animal models. The machine-learning model was trained on a large dataset that we curated. Together, the new system linking these two technologies (Fig. 1) enabled the accurate characterization of all 28 tested drugs and led to the discovery of nine previously unknown transporter–drug interactions. The system also accurately identified the transport profile of 22 investigational compounds, highlighting the relevance of such effects for future drug discovery and development. We validated seven of the newly identified substrate relationships in vivo, supporting the predictive capacity of our efficient and cost-effective system. Moreover, we tested the clinical relevance of novel drug–drug interactions identified through our system and validated four novel drug–drug interactions that led to significantly higher drug levels in patients. Taken together, the system couples machine learning and primary tissue engineering to enhance drug discovery and development by accurately predicting transporter–drug interactions.

Results

Establishing the transportome inter-connectivity

To understand the potential for a drug to be transported by multiple transporters, we first evaluated the incidence of known drug transporter pairs with shared substrates. To this end, we extracted all drug

transporter data from the DrugBank[35] database and analysed the individual transporters according to their shared substrates. DrugBank 5.0 contains 149 distinct drug transporters that have a total of 917 annotated substrates (Fig. 1a). The three transporters with the highest number of annotated substrates are the three efflux transporters P-glycoprotein (P-gp, 186 substrates), breast cancer resistance protein (BCRP, 70 substrates) and multidrug resistance protein 2 (MRP2, 43 substrates), and a total of 106 substrates are partially or fully shared between them (Fig. 1b). Overall, the DrugBank dataset contains a total of 1,891 transporter–transporter interactions, that is, pairs of transporters that have at least one shared substrate. This corresponds to 17% of the possible number of interactions, which shows that shared substrates are a common phenomenon but at the same time do not impact every possible transporter pair. This further shows that transporters possess a complex molecular recognition mechanism of substrates[36,37] and emphasizes the need to develop advanced technology that enables the rapid and accurate profiling of these transporter–drug interactions.

A small interfering RNA-engineered ex vivo system enables the characterization of substrate transport in response to modulation of drug transporter expression

The drug transporters expressed within the small intestine have been studied extensively[7,38,39]. Briefly, three efflux transporters (P-gp, BCRP and MRP2) and three influx transporters (MCT1, SNAT2 and PEPT1) are expressed on the luminal side[38,40]. The basolateral side contains one efflux (ABCC3), one influx (OCT1) and one bi-directional transporter (OSTα/β) (Supplementary Fig. 1a). We hypothesized that porcine tissue could be a viable model system to study these drug transporters given the similarity in gastrointestinal physiology between humans and pigs[26] and the large degree of genetic homology between their drug transporters (Supplementary Fig. 1b). We confirmed a high similarity in the transporter expression levels between porcine and human small intestine tissue through reverse transcription polymerase chain reaction (RT-PCR; Supplementary Fig. 1c) and western blotting (Supplementary Fig. 1d), except for ABCC3 and OSTα/β for which lack of available antibodies prohibited further analysis. In addition, other researchers have shown that first-pass metabolic enzymes are similarly expressed in humans and pigs[41–43], which has established native porcine intestinal tissue as a workhorse in oral drug delivery research[31,44].

To establish a drug transporter model using porcine small intestine tissue, we developed a small interfering RNA (siRNA) knock-down protocol for each transporter in our ex vivo culture system[28]. We designed siRNAs to target all major intestinal transporters and validated their knock-down capacity and specificity first in vitro using the porcine PK15 cell line (Supplementary Fig. 2). This preliminary screen was performed to select siRNA sequences with the best knock-down efficiency. Subsequently, the capacity of these selected siRNAs to knock down their respective transporters after using ultrasound-mediated delivery to our ex vivo culture system was validated[45,46] (Fig. 2a and Supplementary Figs. 3 and 4), and tissue viability, histologic analysis and permeability analysis through transepithelial resistivity measurement as well as permeation evaluation were evaluated to confirm the absence of toxicity from ultrasound (Supplementary Fig. 5). This workflow enabled us to specifically target each drug transporter in the pig small intestine with a knock-down efficiency of twofold to tenfold while not impacting the expression of other transporters as validated through quantitative PCR (Q-PCR; Supplementary Fig. 5a) and western blotting (Supplementary Fig. 5b).

As our ex vivo system retained the intestinal submucosa, we were not able to study basal transporters directly; therefore, we chose to focus our investigation on the luminal drug transporters P-gp, BCRP, MRP2, PEPT1, and MCT1. If a molecule is transported by a specific transporter, its movement across the tissue should be impacted by selectively down regulating that transporter. To validate that our system accurately captures this behaviour, we tested a total of 23 known transporter–drug relationships[7,47]. All investigated drugs showed a significant change in perfusion when their respective transporter was knocked down (Fig. 2b–d and Extended Data Fig. 1; $P < 0.05$, one-tailed Z-test; $P < 0.01$, two-tailed t-test with the exception of Rosuvastatin $P = 2\%$). As a control experiment, we measured the change in perfusion for 11 drugs that are known to not be transported by these transporters[7,48,49] and found that none of their perfusions was significantly affected (Fig. 2b–d and Extended Data Fig. 1; $P > 0.05$, one-tailed Z-test) as expected.

Next, we studied perfusion of drugs that are known to be substrates for multiple transporters to enable the direct validation of our system to study the transportome of small molecules. Down regulating a single transporter did not impact drug perfusion in this case (Fig. 2), hinting at potentially synergistic and compensatory effects in the transportome network. To be able to delineate such effects, we aimed at down regulating multiple transporters simultaneously. We co-delivered two siRNAs targeting P-gp and BCRP with varying concentrations of each siRNA and noted that we were able to fine tune expression levels in a dose-dependent, linear fashion (Pearson $r = 0.72$ and 0.96, Fig. 2e–f). We next studied how the simultaneous and gradual down regulation of transporter expression impacts drug perfusion. Perfusion of BCRP-specific substrates increased linearly with reduced BCRP expression (daunorubicin $R = 0.7$, 4-methylumbelliferone sulfate $R = 0.81$) but were not affected by altering P-gp expression ($P > 0.28$ one-tailed Z-test at maximum siP-gp concentration; Fig. 2g). For substrates of both transporters, down regulation of either individual transporter did not impact perfusion or only marginally at maximal siRNA concentration (Fig. 2h); however, even slight down regulation of both transporters strongly increased drug perfusion up to 160% or 300% (Fig. 2h). These data highlight the ability of this system to capture

Fig. 2 | Validation of the ex vivo drug transporter–drug interaction screening system. a, Schematic of the tissue engineering workflow. **b**–**d**, About 300 µl of 1 µM siRNA (in PBS) targeting P-gp (**b**), BCRP (**c**) and MRP2 (**d**) delivered to individual wells of the intestinal explant system through ultrasound. The fold increase of drug absorption is measured by either fluorescent reading or ultraviolet–visible absorption. For each drug, the data are collected from 62–72 trials ($n = 62–72$) of tissue in four different pigs ($m = 4$). P values were determined by one-tailed Z-test. * $P < 0.05$, ** $P < 0.01$, *** $P < 0.001$. Lines indicate mean value, and error bars correspond to one standard deviation. See also individual raw data plot in Extended Data Fig. 3. **e**, Western blotting against P-gp and BCRP shows that the expression levels of the drug transporters are correlated with the concentration of dosed siRNA in the range of 0 to 25 µM. Same blot is also processed for loading control protein β-actin for quantitative analysis. **f**, A representative western blot; the relative expression level of each target after siRNA dosing is calculated using the band density ratio compared to control on a single image taken from one gel without further processing using ImageJ, and multiple gels have been prepared in parallel to arrive at replicates. The original image for each western-blot gel can be found in Supplementary Fig. 12. **g**, The relationship between fold increase in perfusion for BCRP-specific substrates daunorubicin and 4-methylumbebeliferone sulfate and the level of BCRP expression. The expression level of BCRP is calculated by western blot as shown in **f**, and the experiments were repeated for at least three times. The same analysis method was performed for each individual replicate to obtain statistical significance. **h**, The relationship between fold increase in perfusion of substrates (doxorubicin and topotecan) that are transported by two efflux transporters (P-gp and BCRP) and the expression level of each individual drug transporter when dosed with single siRNA. The green line indicates the relationship between fold increase of doxorubicin and topotecan to the expression level of P-gp and BCRP when co-dosing siP-gp and siBCRP with different concentrations. Data for **f**–**h** are pooled from three independent experiments. Lines indicate mean value, and error bars correspond to one standard deviation.

https://doi.org/10.1038/s41551-023-01128-9

the dynamic interplay and synergistic effects of multiple transporters that can compensate the loss of one of the two transporters.

Development of a machine-learning model for the rapid prediction of transporter–drug profiles

While our data indicated that we are able to knock down a set of transporters to study the transporter profile of clinically relevant drug molecules, the combinatorial explosion of necessary experiments prohibits exhaustive profiling. For example, investigating the full transportome profile for a single drug by creating all possible knock-down combinations of the 149 known drug transporters would require more than 700 tredecillion (7×10^{44}) experiments. Given the established role of machine learning to streamline experiments, we set out to test whether a classification model could prioritize knock-down experiments. We first validated that the 'chemical similarity principle' holds in our dataset by comparing the average nearest neighbour Tanimoto similarity of transporter substrates (0.53 ± 0.24) and their similarity to non-substrates (0.39 ± 0.18), which indicated that substrates share

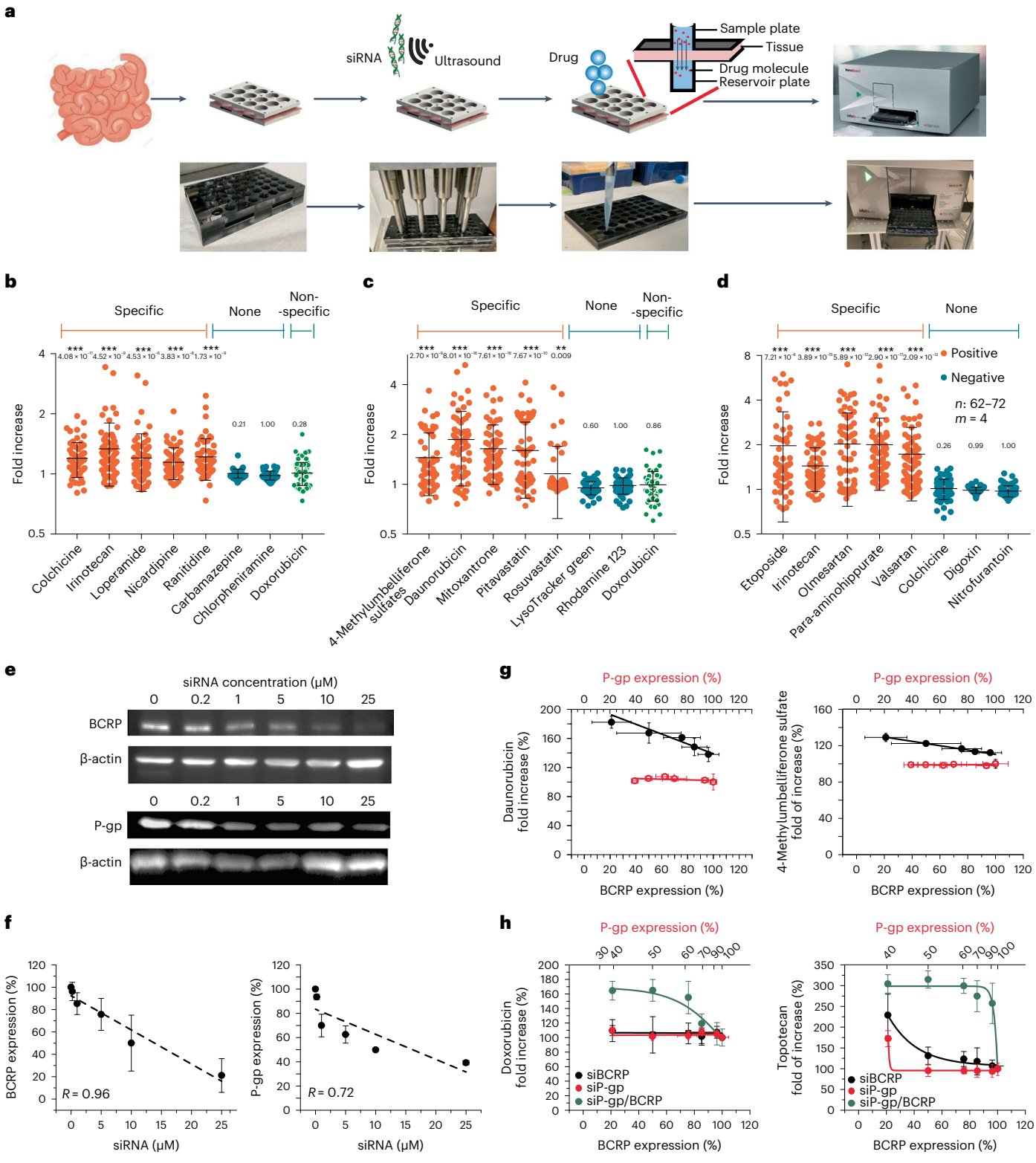

significantly higher chemical similarity (unpaired Student's *t*-test $P = 3 \times 10^{-58}$) that can be exploited to model the transporter–drug relationships (Supplementary Fig. 6a). Principal component analysis showed that transporter substrates occupy specific regions in chemical space (Supplementary Fig. 6b).

We specifically aimed to design a machine-learning model with maximal specificity (that is, high true negative rate) as such a model would enable the accurate identification of non-substrate relationships, thereby preventing testing of non-substrates and preserving resources. High sensitivity (that is, high true positive rate) was not required as our ex vivo system eliminates any false-positive predictions. We concentrated our machine-learning efforts on the three efflux transporters P-gp, BCRP and MRP2 given their significance for clinical drug transport as supported by having the greatest number of annotated substrates (Fig. 1a). We manually curated a training dataset mined from DrugBank[35], Metrabase[50] and the National Institutes of Health (NIH) screen NCI-60 (refs. 51,52). A random forest machine-learning model showed the highest specificity of up to 96%, indicating that it can accurately identify non-substrates to streamline experimental testing (Supplementary Table 1). We confirmed that the random forest architecture outperforms seven other machine-learning models trained on our data (Supplementary Fig. 7 and Supplementary Table 1), potentially due to the need for additional parameter optimization for other models or the lack of implicit feature selection except for tree-based learning approaches which performed best. As expected, adversarial Y-shuffling broke the relationship between chemical patterns and substrate relationships and therefore collapses the model (Supplementary Table 2), and data ablation reduces model performance (Supplementary Table 3). We also refuted that the high performance is exclusively driven by analogue identification by showing that the model retained high precision in cluster-based cross validations (Supplementary Table 4). We recognized that our training data were slightly imbalanced and therefore tested the potential of 17 machine-learning techniques to augment our model for imbalanced data. None of these learning techniques improved the specificity of our model (Supplementary Fig. 7 and Supplementary Table 5). An analysis of the relative feature importance for these models highlights the importance of physicochemical properties of small molecules to predict substrate relationships. This analysis also shows the need to consider different properties to make accurate predictions for the different studied transporter proteins (Supplementary Table 6).

To assess the performance of our model on external data, we predicted unknown transporter–drug relationships for our training molecules, thereby completing the transporter profiles for compounds that are only partially annotated in our data. We then manually screened the literature to validate or refute these predictions. Overall, 70% of these predictions were validated to be correct (Supplementary Table 7), where 58% were correct transporter–drug interactions, while 42% were correct predictions of non-substrates. The ratio of substrates to non-substrates was much higher in the literature compared to the databases that we used, possibly hinting at reporting biases for positive results in the literature. The high performance of our model on these external data showcased the capability of our model to correctly identify both substrates and non-substrates even in cases where the underlying class distribution was distinct from the training data. We noted that accuracy correlated with predictive confidence (percentage of trees in our random forest ensemble that predict the molecule to be a substrate), with 80% of the high-confidence predictions being correct, while only 50% of low-confidence predictions were correct. This indicated that a confidence cut-off of 60% would allow us to define an applicability domain of our model with largely correct predictions, while predictions with lower confidence were insufficiently understood. Conversely, insufficiently understood compounds provide an opportunity for model augmentation, as such poorly understood compounds can be expected to add knowledge to the model. We therefore followed an active learning strategy to specifically annotate predictions with low confidence to generate an augmented dataset of 4,554 transporter–drug relationships (Supplementary Table 8).

Machine learning and tissue engineering streamline the identification of substrate relationships for approved drugs and investigational compounds

We first aimed to assess whether our model could generate useful insights for approved drugs. To this end, we applied our machine-learning model based on the 4,554 transporter–drug relationships dataset to a panel of 28 model drugs that form a representative set of molecular structures with a wide range of intestinal perfusion abilities[28]. We exhaustively screened their transporter interactions with P-gp, BCRP and MRP2 through knock-down experiments. Overall, we found that machine learning and the experimental results agreed in 76.2% of the experiments, indicating that the rapid in silico predictions enable experimental streamlining. As these approved drugs are established medications that have undergone ample pre-clinical and clinical investigation, we noted that half (57.1%) of their transporter interactions can be found in the literature. This attests to the ability of our workflow to detect relationships that can also be identified via classical experimental and clinical workflows. Notwithstanding these previous efforts, our focused screen of 28 model drugs discovered 9 currently unknown transporter–drug interactions that had not been reported previously (Supplementary Table 9), suggesting that our system can generate new transporter knowledge even for highly scrutinized molecules. Importantly, these findings could have immediate implications for patients receiving these medications.

Given these promising results for established medications, we next determined whether the system could also discover transporter profiles for investigational drugs. After adding the drug screening data to our database (Supplementary Table 8), the system predicted the transporter profile of 1,595 investigational, small-molecule drugs (DrugBank 5.0). Using these predictions, we classified all investigational drugs into eight categories: selective substrates for either P-gp, BCRP or MRP2; dual substrates for either P-gp/BCRP, P-gp/MRP2 or BCRP/MRP2; 'super substrates' that are substrates for all three drug transporters; and 'super drugs' with no predicted interaction and therefore no transport liability. We then selected the top three hits from each of these eight categories (with the exception of the P-gp/MRP2 dual substrate gallopamil, given the commercial unavailability of the other top candidates), resulting in a validation set of 22 compounds that we tested experimentally for their predicted transporter interactions. About 91% of our predictions were validated ex vivo (Fig. 3), covering all possible classes of transporter profiles. This confirmed the applicability of our workflow to preclinical drug development and also further attests to the ability of the system to identify distinct types of transporter profile.

Feedback loop enables applicability domain expansion

As we had gone through multiple iterations of predictions and data generation with novel data added to the model, we set out to characterize the impact of these data to the model. We tracked five-times stratified tenfold cross validation as well as out-of-bag error performance of all our models (Supplementary Tables 10 and 11). The directed data augmentation through active learning led to slight improvements in sensitivity for all models while maintaining high precision. This could indicate that adaptive data augmentation can specifically improve weaknesses of a model according to certain performance characteristics. The other screening data did not alter model performance, corroborating previous results that inclusion of high-confidence predictions does not positively impact machine-learning models[53,54]. However, as all models are evaluated on distinct datasets, a direct comparison might not be a true reflection of their relative predictive power. We quantified

https://doi.org/10.1038/s41551-023-01128-9

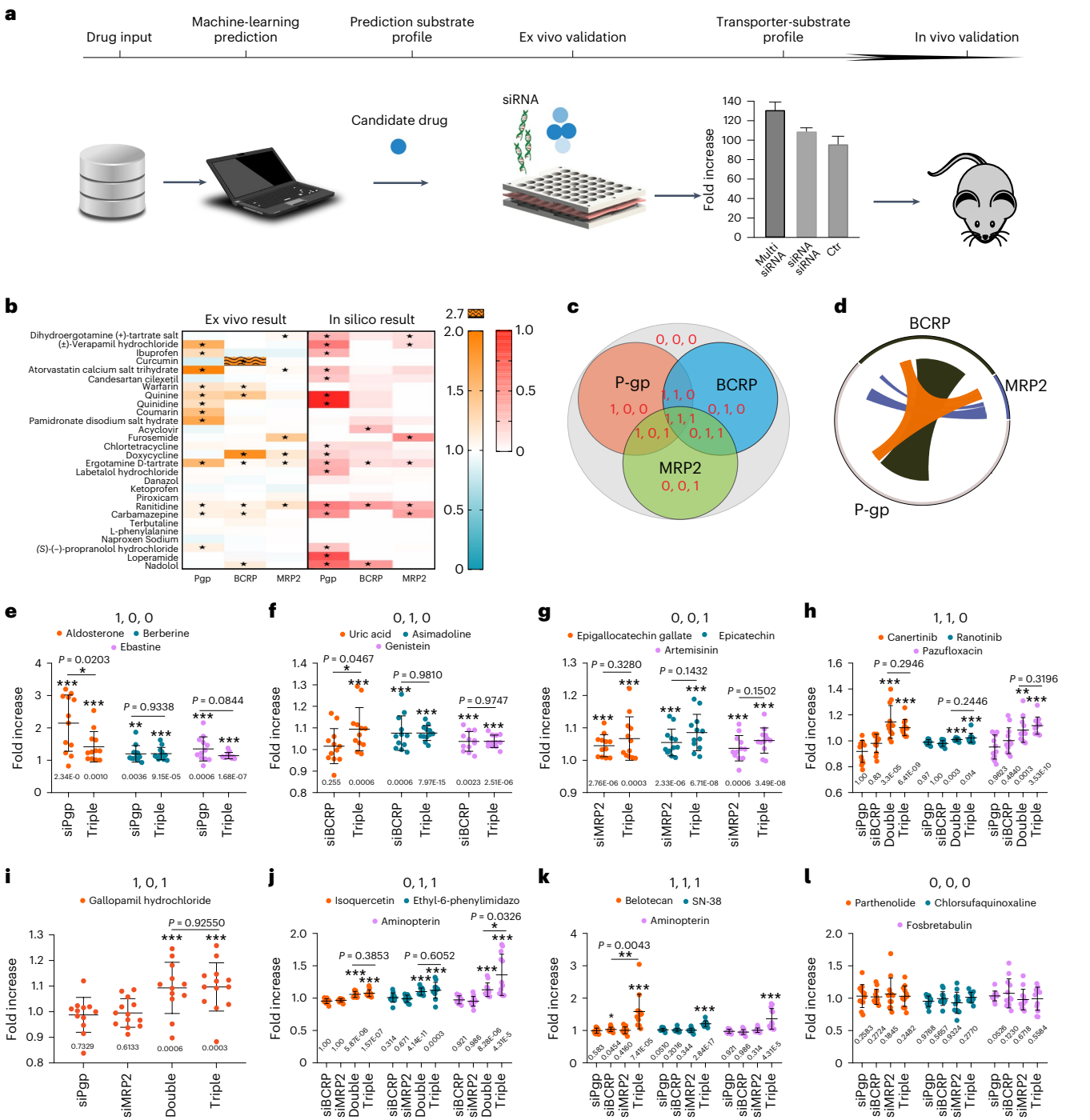

Fig. 3 | In silico and ex vivo prediction and validation of drug–drug transporter interactions. a, Schematic of the combined workflow. Substrate data were curated and provided to the machine-learning algorithm. This algorithm was then used to predict drug transporter–drug interactions. Predictions were then subsequently validated on the ex vivo system by delivering the respective siRNA(s) via ultrasound to the porcine explant system. Top predictions are then further validated in vivo. **b**, Heat map of the fold increase of perfusion (left) upon drug transporter knock-down (P-gp, BCRP and MRP2, respectively) and confidence in potential transporter–drug interaction prediction (right) for 28 commercial drugs. An asterisk indicates a statistically significant increase in perfusion (left) or a predictive confidence >50% (right). **c**, Schematic of the different prediction categories considered here and described as binary code. In this code, 0 indicates a non-interaction, and 1 corresponds to interactions; the position of the number indicates the specific transporter, whereas the first number indicates P-gp interactions, the second number indicates BCRP interactions, and the third number signifies the interaction with MRP2. **d**, Chord plot visualizes the predicted transporter–transporter relationships. Circle fraction is indicative of relative number of substrates per transporter. Shared substrates are connected through proportional surfaces. **e**–**g**, Fold increase in perfusion of top drugs that were predicted to interact with only one drug transporter when dosing predicted single siRNA (i.e., siP-gp in panel (**e**), siBCRP in panel (**f**), and siMRP2 in panel (**g**)) and triple siRNAs, respectively. **h**–**j**, Fold increase in perfusion of top drugs that were predicted to interact with two drug transporters when dosing single siRNA, two siRNA combined and triple siRNAs, respectively (i.e., siP-gp/BCRP in panel (**h**), siP-gp/MRP2 in panel (**i**), and siBCRP/MRP2 in panel (**j**)). **k**,**l**, Fold increase in perfusion of top drugs that were predicted to interact with all three (**k**) or none (**l**) of the drug transporters when dosing each single siRNA and combined triple siRNAs, respectively. For plots **e**–**l**, the data were collected from 12 trials ($n = 12$) of tissue extracted from three different pigs ($N = 3$). P values for each condition were determined by one-tailed Z-test. P values for comparison between groups was determined by Student's t-test with multiple test correction. * $P < 0.05$, ** $P < 0.01$, *** $P < 0.001$. Lines indicate mean value, and error bars correspond to one standard deviation.

https://doi.org/10.1038/s41551-023-01128-9

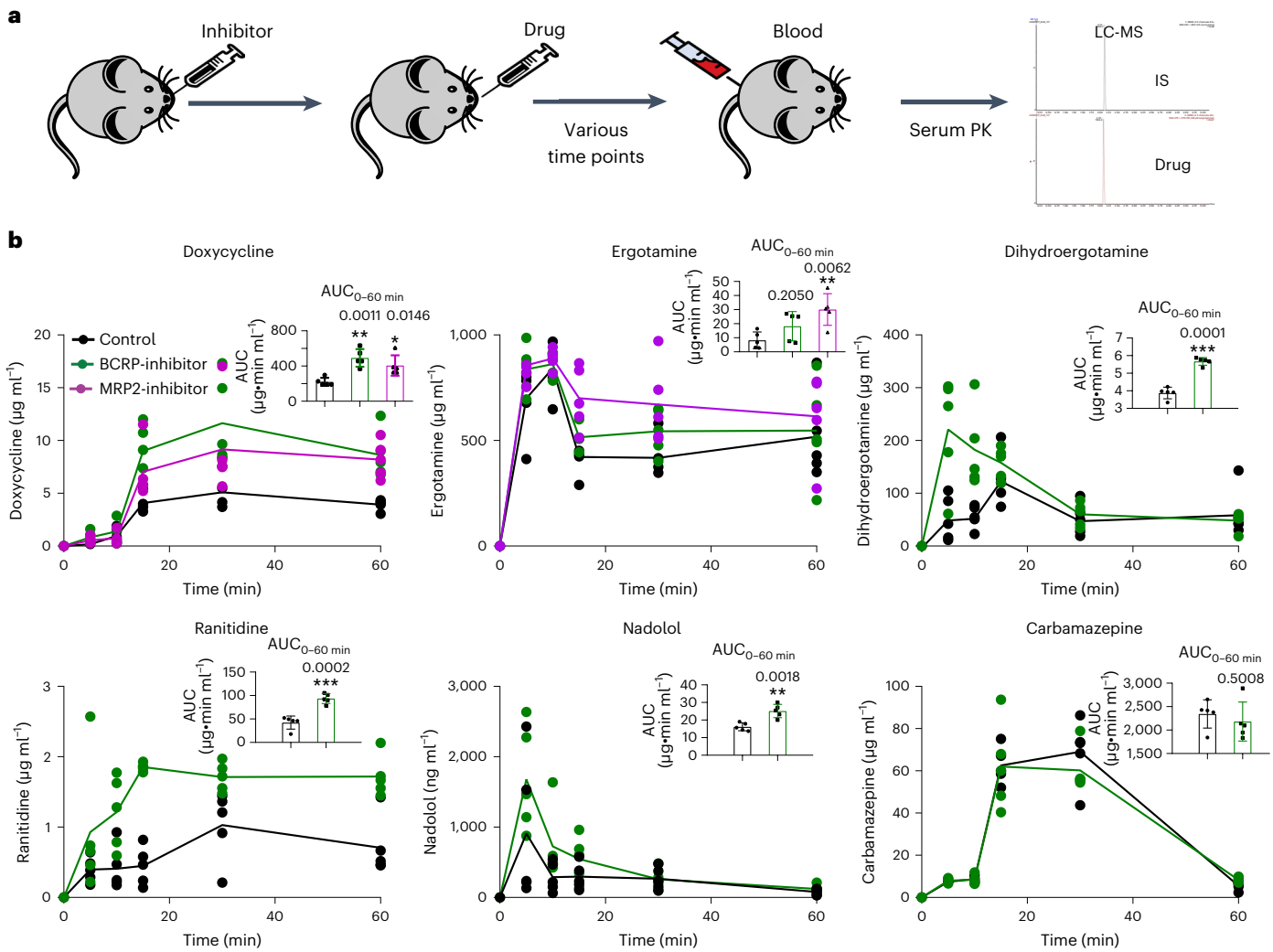

Fig. 4 | Validation of novel drug–transporter interactions in vivo, and prediction, ex vivo discovery and clinical validation of transportome-derived drug–drug interactions. a, Experimental schematic for in vivo validation. IS, internal standard; PK, pharmacokinetics. **b**, In vivo pharmacokinetics of potential substrates identified from Fig. 3 on Balb/c mice. Drug transporter inhibitor (verapamil for P-gp, imatinib for MRP2 and probenecid for BCRP) was administered 15 min before drug via oral gavage, while for the control group, PBS was administered instead. The serum drug level was determined through LC-MS/MS, high-performance liquid chromatography and/or gas chromatography-mass spectrometry. $n = 5$ for each time point. Inserts show AUC comparison within 60 min time window after drug oral administration for potential substrate from **a**. P value was calculated based on one-way analysis of variance. $^{*}P < 0.05$, $^{**}P < 0.01$, $^{***}P < 0.001$.

the number of high-confidence predictions of all models as a measure of applicability domain extension and found that the initial data augmentation expanded the number of high-confidence predictions, while less directed data acquisition strategies did not positively impact model confidence (Supplementary Table 12)—fully corroborating previous results[54]. While the direct integration of machine learning and our experimental system holds potential for improving data acquisition, the continuous accumulation of distinct types of data could further show the value of this integrated model.

In vivo validation of novel transport associations

To validate the physiological relevance of the newly identified substrate relationships, we performed an in vivo pharmacokinetic study in Balb/c mice. Candidate drugs were delivered by oral gavage, and the resulting drug concentration in blood serum was determined for the following 60 min (Fig. 4a and Supplementary Fig. 8) to capture the absorption phase of the pharmacokinetic curve. We compared the area under the concentration–time curve (AUC) when administering the candidate drugs to naive mice compared to mice in which we reduced the function of specific drug transporters by pre-treating the mouse through oral administration of known transporter inhibitors (verapamil for P-gp[55], imatinib for BCRP[56,57] or probenecid for MRP2 (ref. 58)). Analysis of relative AUCs revealed a significant increase in drug absorption for 7 out of the 8 tested candidate drugs ($P < 0.05$, two-tailed Student's t-test; Fig. 4b). Only carbamazepine did not show the expected effect, which might be explained by increased glucoronidation of carbamazepine induced by our transporter inhibitor probenecid[59]. These results support the predictive capacity of our approach and the transferability of acquired results into complex in vivo conditions and showcase our ability to generate actionable knowledge of drug transport liabilities for approved drugs. For example, doxycycline is a known substrate of P-gp and OAT1, but the newly discovered interactions with BCRP and MRP2 double the number of known transporters for this drug.

Identifying transporter-induced drug–drug interactions

We hypothesized that newly identified transporter substrate profiles might not only be relevant to understand and improve individual drug absorption but could also be the cause for clinically relevant drug–drug

https://doi.org/10.1038/s41551-023-01128-9

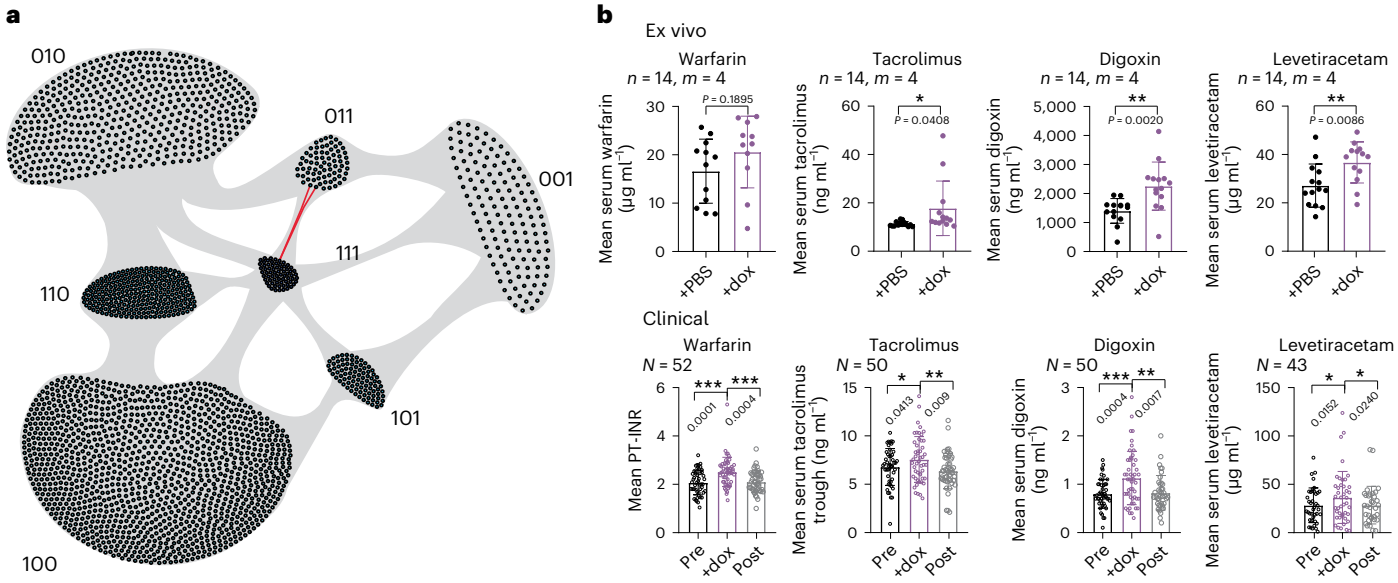

Fig. 5 | Visualization of predicted drug–drug interactions through transportome profiles, and ex vivo validation and clinical data analysis of doxycycline interactions with warfarin, tacrolimus, digoxin and levetiracetam. a, Binary code as in Fig. 3. Drugs are clustered according to their transport profile. All drugs within one cluster are defined as interacting, and two clusters are connected by a grey area if the drugs across these clusters have the potential to interact through (partly) shared substrate relationships. Pairs further investigated are connected by a red line. **b**, The detailed ex vivo experimental procedure is described in Methods. Briefly, warfarin, tacrolimus, digoxin and levetiracetam were co-treated with doxycycline on our ex vivo swine tissue respectively to investigate changes in perfusion of the tested drugs. The tested drug concentrations were determined by LC-MS from the reservoir well. Detailed clinical trial and data analyses are described in Methods. Briefly, in patients (n = 43–50) undergoing warfarin, tacrolimus, digoxin or levetiracetam treatment, there were significant increases in PT-INR, serum tacrolimus trough levels, serum digoxin levels and serum levetiracetam levels, respectively, while a patient received a concomitant short course of doxycycline therapy, and PT-INR/drug levels returned back to baseline after doxycycline clearance. Boxes indicate mean value, and error bars correspond to one standard deviation. * P < 0.05, ** P < 0.01, *** P < 0.001. PBS, phosphate buffered saline; dox, doxycycline; Pre, prior to doxycycline treatment; Post, after doxycycline treatment.

interactions when two medications compete for the same transporter. To gauge the potential magnitude of this challenge, we predicted the P-gp, BCRP and MRP2 substrate profiles for all small molecules found in DrugBank 5.0. We then defined potential drug–drug interactions as pairs of drugs that share at least one known or predicted transporter, given that an overlapping substrate or inhibitor relationship might alter transport kinetics for both substrates. By this definition, newly predicted transporter–drug relationships could cause up to 1,810,270 potential novel drug–drug interactions that were not known based on previously known transporter–drug relationships (Fig. 5a). We realized that some of the substrate predictions had low predictive confidence, indicating a potential for a substantial number of both false-positive and false-negative predictions that might impact the total number of drug–drug interactions. When only focusing on confident predictions (confidence score >60%), we predict 303,626 drug–drug interactions, which corresponds to a tenfold increase over interactions based on currently known transporter relationships.

While these numbers are staggering, it is unknown whether these calculated substrate profiles are indeed predictive of altered drug uptake during co-administration of the identified pairs of drugs. We set out to validate some of the predicted interactions experimentally. We chose doxycycline as the primary test compound given its broad clinical use and that we had here identified and in vivo validated as a novel BCRP and MRP2 substrate (Figs. 3b and 4b). We then manually selected four candidate drugs that are known substrates of BCRP and MRP2 to study whether they could potentially interact with doxycycline. We chose warfarin, tacrolimus, digoxin and levetiracetam as candidates for the following reasons: (1) close monitoring of warfarin through prothrombin time and international normalized ratio (PT-INR) levels and tacrolimus, digoxin and levetiracetam levels in the clinic enables the direct identification of potential interactions from clinical data; (2) they have narrow therapeutic windows which makes the identification of potential interacting drugs critical; (3) a considerable fraction of the patient population receive combinations of these drugs with doxycycline to treat their co-morbidities; and (4) while for tacrolimus there have been previous suggestions of potential interactions with doxycycline without a clearly identified mechanism[60], the other three (warfarin, digoxin, levetiracetam) represent currently unknown interactions with doxycycline. As a first-line test, we conducted ex vivo perfusion experiments to test for changes in absorption when co-administering the candidates with doxycycline. All drugs except warfarin showed a significant increase in perfusion upon co-treatment with doxycycline (Fig. 5b; P = 0.19, 0.041, 0.002 and 0.009).

To assess the clinical relevance of these findings, we identified patients (n = 43–50) from the Mass General Brigham Research Patient Data Registry (RPDR) for which we could acquire data on their drug levels before, during and after doxycycline administration. We found a significant increase of all four tested drugs when co-administrated with doxycycline (P = 0.0001, 0.0413, 0.0004 and 0.0152), while levels returned to baseline after completion of doxycycline therapy (P = 0.0004, 0.009, 0.0017 and 0.024). We next modelled the effect of doxycycline concentration on the absorption of the interacting drugs with biopharmaceutical modelling. Due to the limited information available about the receptor kinetics of doxycycline and BCRP except that of digoxin, we were only able to estimate digoxin's maximal increase in serum concentration expected with inhibition of BCRP. Our modelling results suggested that the complete inhibition of BCRP can increase serum concentration of digoxin by ~62% (Supplementary Results and Supplementary Fig. 9), which is in good alignment with ~50% increase in average serum concentrations in our retrospective clinical study. Although warfarin and tacrolimus are also metabolized through cytochrome P450 3A4, which might at least in part explain

this interaction, digoxin and levetiracetam are not cytochrome substrates or share any other known metabolic enzymes with doxycycline. Although we cannot exclude that other unknown enzymes may play a role in this drug–drug interaction, we believe that the clinical data combined with our ex vivo data provide good evidence for transporter-driven interactions. Importantly, with the exception of a moderate clinical warning for doxycycline–warfarin, none of the other combinations are currently recognized as known drug–drug interactions. Therefore, these cases highlight the potential of our system to identify clinically relevant and previously unknown drug–drug interactions with immediate implications for clinical practice.

Discussion

Drug transporters can be major determinants of the absorption, kinetics and elimination of life-saving therapeutics. It is currently underrecognized that drugs are substrates for multiple drug transporters, leading to complex transporter–drug interaction patterns that can drastically reduce bioavailability[61,62], increase the risk of drug resistance[63] and exponentially increase the number of drug–drug interactions[64,65]. Our data suggest that complex transport profiles involving more than one transporter are in fact common among both approved and investigational drugs (compare Figs. 1a,b and 3d). Therefore, understanding the effects of multiple drug transporters on a single compound and characterizing the transportome is critical for preclinical drug development and clinical decision making.

We have here directly integrated machine learning with a screening system based on genetically engineered ex vivo tissue. Through direct integration, the machine-learning algorithm can prioritize experiments while adaptively learning from the continuously acquired data. Through genetic engineering, we enabled the characterization of multi-transporter effects in a complex tissue context. Our data suggest that compensating effects of multiple transporters can obscure individual transport interactions (Figs. 2h and 3h–k), which highlights the need for new experimental systems and provides an important caveat for a large fraction of the currently available substrate data that have been largely derived from simple model systems that do not take compensatory effects into account.

Our machine-learning model enabled us to streamline experiments with high precision but low sensitivity. We identified that a portion of the false predictions were likely occurring as a result of complex biological effects, such as additional drug–drug interactions between the tested drug carbamazepine and the control inhibitor probenecid. Another major reason for the false predictions might be caused by different experimental conditions under which the training data had been generated. Such changes in protocols can lead to different interpretations and thereby to conflicting information provided to the model. Tight integration of experiments and machine learning will serve to circumvent at least some of these challenges. In future, we expect that our system and other experimental set-ups can provide more detailed kinetic information, such as Michaelis–Menten constant (K_m) values, which could further boost predictive power and the translational relevance of the approach.

Although the used tissues showed variation in siRNA efficiency and drug perfusion, as expected, and the observed fold changes were not direct measurements of pharmacokinetic differences in vivo, we confirmed that our system provides physiologically relevant data, with all 24 drugs with clinically relevant transport profiles showing the expected behaviour (Fig. 2b–d) and with 87.5% concordance of our predictions in the in vivo Balb/c mouse model (Fig. 4). Nevertheless, inter-species differences in substrate relationships and enzyme homology will continue to pose important challenges for work in this area. In the future, bypass surgeries and donors might provide access to human tissue, which could circumvent species differences, enable the detailed analysis of personal variations[66] and generate important data for personalized drug delivery. Similarly, interactions of additional transporters and other metabolic enzymes across different tissues will have to be integrated in future systems. With increasingly available data, tissue and genetic tools, we expect to expand our system to other enzymes, organs and pathways.

Our ability to rapidly identify clinically relevant drug interactions from millions of possible pairings hints at the potential power of the described system and extensions thereof, which could be easily and rapidly deployed into current drug discovery, development and delivery pipelines. Approaches such as this show that combinations of technologies including machine learning and tissue engineering can accelerate drug and formulation development by prioritizing drug candidates and formulations while mitigating the risks of the development of drug resistance and of unexpected drug–drug interactions.

Methods

Transportome interaction graph

DrugBank 5.0 was downloaded in XML format, and all DrugBank entries with at least one known transporter were extracted in Python 2.6. For every such entry, the list of known transporters per entry was extracted and stored in a numpy array. These lists were then processed to identify the total number of substrates per transporter and the number of shared substrates per transporter pair, which were converted into an adjacency matrix and imported into Gephi 0.9.2. In this graph, every node corresponds to a drug transporter, and two nodes are connected if and only if the corresponding two drug transporters share at least one known substrate according to DrugBank 5.0. The node size was determined from the total number of known substrates per transporter, using a logarithmic interpolation to ensure visibility of all nodes. Edge thickness was determined from the number of shared substrates and scaled linearly. Node position was determined using the Fruchterman Reingold layout algorithm. Chord charts to highlight the substrate sets for P-gp, BCRP and MRP2 were generated using the R library circlize and further processed in Inkscape (v.0.92).

Transport database

Data for human transporter substrates were extracted from Drugbank 5.0 and Metrabase 1.0 and from the NIH screen NCI-60 for P-gp, BCRP and MRP2. All these datasets provide independent, expert curated, binary class data on the substrate/non-substrate relationships for the investigated transporter. The data were not further filtered for specific experimental protocols or readouts. Annotations were removed if contradicting information was present within one database. For the NIH screening data, we followed previously published and validated protocols to correlate treatment efficacy of various cytotoxic drugs against different cell lines with drug transporter expression levels for these cell lines. Briefly, if there is a sufficient anti-correlation (Pearson correlation coefficient less than −0.2) between transporter expression levels and cytotoxic effects of the compound, the compound is assumed to be a substrate of the transporter under investigation; otherwise it can be assumed not to be transported by the specific transporter. To reflect our confidence in the annotations, we prioritized annotations in DrugBank over Metrabase annotations, and we prioritized DrugBank and Metrabase annotations over data extracted from the NIH screen NCI-60. Compound identity was determined using a Morgan fingerprint (2048 bits, radius 4) with a Tanimoto similarity threshold of 0.95. For initial data augmentation, we used our Random Forest machine-learning model based on these data to predict the missing annotations, that is, substrate relationships for compounds that were included because of their relationship to other transporters. Manual literature research for randomly selected predictions showed that 70% of the high-confidence predictions (substrate probability score >60% or <40%) were correct, while only half of the low-confidence predictions (40% < substrate probability score < 60%) were correct. We followed an active learning strategy to manually augment the dataset for these low-confidence predictions by comprehensively scanning

the literature for more information on compounds that were predicted with low confidence and annotate them in our dataset. This led to our larger, augmented training dataset. After screening of our model drug library, we considered all drugs with statistically significant changes in perfusion to be substrates of the investigated transporters, and these data were subsequently added to the third generation of our database. The final results for the investigational drugs were subsequently added in the same manner. The number of substrates/non-substrates in these datasets are included in Supplementary Table 8, and the performance of models trained on these datasets is reported in Supplementary Tables 10 and 11.

Machine-learning model

Compounds from the training database were described using Morgan fingerprints (radius 4, 2,048 bits). The machine-learning model was a Random Forest Classifier (scikit-learn) using 500 tree estimators and no threshold on the number of included descriptors. Model quality was estimated retrospectively using five-times stratified tenfold cross validation with pre-shuffling to ensure randomization of training and test sets. For model comparison, we also implemented Gaussian naive Bayes, kNN ($k = 3$), a decision tree, a multilayer perceptron neural network, a linear support-vector machine and extra randomized trees (all scikit-learn with default parameters). In addition, we implemented two deep models: a Message Passing Neural Network and Path-Augmented Graph Transformer Network (both DeepChem with default parameters). For cluster-based cross-validation, we used k-means ($k = 50$) clustering based on Molecular ACCess Systems (MACCS) key fingerprints (rdkit v.2020.09.1) to group our database and perform leave-one-cluster-out cross-validation (scikit-learn v.1.0.2). In addition, we tracked out-of-bag errors of our random forest models on the different databases. We also tested the integration of class-based instance weighting (scikit-learn) and of all 16 up-sampling and down-sampling strategies in the Python imblearn library to further improve the performance of our models, but none of these imbalanced learning techniques improved the specificity of our model (Supplementary Table 4).

Prediction of investigational drugs

Investigational drugs were extracted from DrugBank by selecting compounds categorized as investigational but not in any of the other categories (for example, approved or withdrawn), and compounds that were part of the training set were eliminated. This led to a total number of 1,594 investigational drugs with unknown transport profiles. Using our machine-learning model, we predicted the confidence score for each of these compounds to be transported by P-gp (s1), BCRP (s2) or MRP2 (s3). The confidence of a substrate prediction was calculated as the number of trees predicting the molecule to be a substrate divided by the total number of trees in our random forest ensemble. A molecule was predicted to be a substrate if it has a confidence score of at least 50%; otherwise it was predicted to be a non-substrate. This resulted in three confidence scores s1, s2 and s3, each ranging from 0.0 to 1.0. We then ranked compounds according to how closely their predicted transport profile (s1, s2, s3) would resemble any of the $2^3 = 8$ different idealized profiles, specifically drugs that would not be transported by any of the three transporters (0, 0, 0); selectively transported drugs (1, 0, 0), (0, 1, 0), (0, 0, 1); drugs that would be transported by any pair of investigated transporters (1, 1, 0), (1, 0, 1), (1, 1, 0); and drugs that were predicted to be transported by all three transporters (1, 1, 1). By utilizing the Euclidean distance between the predicted profile (s1, s2, s3) and any of these idealized profiles, we generated a total of $1{,}594 \times 8 = 12{,}752$ rank scores.

Cell culture and short hairpin RNA and siRNA transfection

The *Sus scrofa* kidney epithelial cell line PK15 was gifted by George Church's lab at Harvard University and cultured in Dulbecco's modified Eagle's medium (DMEM, Invitrogen), high glucose supplemented with 10% fetal bovine serum (Invitrogen) and 1% penicillin/streptomycin (Invitrogen), as suggested by the commercial protocol. Cells were maintained at 37 °C in an incubator with 5% CO_2 supplement. Short hairpin RNA and siRNA transfection was delivered into PK15 cell by standard lipofectamine 2000 kit (Invitrogen) according to the manufacturer's protocol.

Tissue dissection and preparation

Pig tissue was sourced from local slaughterhouses (that is, Leman & Sons, Hilltown Pork and Blood Farm). Tissue was procured from domestic pigs (*S. scrofa*) that were 6 months old and had a body weight between 140 lb and 200 lb. The tissue is prepared according to previous described protocols[28]. Briefly, the jejunum of the small intestine tissue was isolated from the intact gastrointestinal tract immediately after euthanasia and dissected longitudinally. The tunica muscularis was removed and the tissue sliced into pieces of approximately 150 mm in length. Tissue that contained Peyer's patches was eliminated in this study. A series of washes with PBS supplemented with 5% antibiotic–antimycotic solution (Thermo Fisher Scientific) was applied to the tissue until clean under sterile conditions. Then, the tissue was mounted on the GI tissue robotic interface system (GI-TRIS) filled with a PBS 5% antibiotic–antimycotic solution and cultured at 37 °C incubation with 5% CO_2 supplement. The tissue dissection and preparation were performed within 30 min and immediately submitted for siRNA treatment as described below.

Ultrasound siRNA delivery

siRNA duplex solution (that is, P-gp, BCRP, MRP2, SNAT2, Pept1, MCT1, OSTa and ABCC3) was diluted into PBS solution to a final concentration of 1 µM. For a 48-well GI-TRIS, 300 µl of siRNA solution was added into each well, and the siRNA was delivered to tissue through a 12-head 40 kHz ultrasound device by applying 5 s intervals for 1 min with 30% amplitude as previously described[45,46]. Tissue was cultured for 24 h before the perfusion assay. We confirmed viability and integrity of the tissue using standard assays of cell viability, ATP and histology, and by measuring perfusion of dextran and transepithelial/transendothelial electrical resistance (TEER) before and after the ultrasound treatment (Extended Data Fig. 1).

Western blotting

Tissue was dissected and snap frozen in liquid nitrogen. Every 1 mg of tissue sample was homogenized in 100 µl of RIPA buffer supplied with protease inhibitor (Roche) by Berkin 24-cycle homogenizer. After centrifugation, the protein concentration from the supernatant was determined by BCA assay (Pierce) according to the manufacturer's protocol. A total of 100 µg of protein was loaded on each lane for western blotting. The primary and secondary antibody working concentration is summarized in Supplementary Table 13. Blots were imaged with Bio-Rad Universal Hood II Molecular Imager (1312M) with chemiluminescence method. Contrast setting was set to auto-contrast for all images.

GI-TRIS design and manufacture

A 48-well GI-TRIS for interfacing with explanted porcine small intestine was designed and fabricated based on modifications from previous work[28]. The device consists of a bottom reservoir plate and an upper load plate. Both plates were made by laser cutting (Universal Laser Systems VLS6.60) a standard 48-well plate outline and well pattern (Corning 48-well plate, transparent) as well as magnet holes onto an acrylic sheet (McMaster–Carr 1/4 inch thickness). Neodymium magnets (K&J Magnetics Cylinder, 3/16 inch × 3/16 inch, N52, NI) were press fitted into the magnet holes of both plates. Seal film (Thermo) was applied to seal the bottoms of the wells of the reservoir plate, and PBS solution was loaded into each well. Then, tissue was placed on top of the reservoir plate, and the upper load plate was laid on top of the tissue. The magnets were oriented to align and attract the two plates

together, ensuring a strong seal between the wells. The concept demonstration of the device is shown in Fig. 2a. Design details are provided in Supplementary Fig. 3.

Drug preparation, perfusion and detection

For the ex vivo perfusion study, the detection of each drug is based on either fluorescence or absorbance measurements according to the literature. A 1 mg ml^{-1} drug stock was prepared for each drug in PBS (pH 7.4). For water-insoluble drugs, a final concentration of DMSO in PBS was used to solubilize drugs. We centrifuged samples before further testing to remove any insoluble residues. Absorbance measurements confirmed the absence of any large aggregates (Supplementary Fig. 10). Drug solutions were then added to the tissue, and we measured perfusion after 1 h incubation as described in a previous publication[28]. We quantified perfusion through measurement of standard curves (Supplementary Fig. 11) and ensured that the detected drugs are in the linear range of the calibration curves. 'Fold increase' was defined as the ratio of amount of perfused drug through siRNA-treated tissue to amount of drug perfused through non-treated tissue (PBS control). Therefore, a fold increase of 1 indicates no difference in drug perfusion and therefore no role of the transporter. A detailed drug list, preparation methods, and detection parameters is summarized in Supplementary Tables 9 and 14–17.

In vivo pharmacokinetic analysis of predicted drug transporter substrates

All animal procedures were conducted in accordance with protocols approved by the Massachusetts Institute of Technology Committee on Animal Care. For in vivo pharmacokinetic evaluation, female Balb/c mice aged between 10 and 12 weeks were used in this study. For each studied drug, two groups were included, with three time points (15, 30 and 60 min)—each time point contained five mice for each group. The control group was designed to obtain a baseline of absorption for the investigated drug in which no specific drug transporter inhibitor was used. For the experimental group, drug transporter-specific inhibitors were pre-administered through oral gavage 15 min before the administration of the investigated drugs. For each time point, 1 ml of blood was drained from the mice after oral gavage administration. The blood was further treated by centrifugation, then by protein precipitation with acetonitrile in preparation for liquid chromatography tandem mass spectrometry (LC-MS/MS) analysis.

RT-PCR and Q-PCR

RNA from cell and tissue were extracted with the Trizol extraction method and converted into complementary DNA according to the manufacturer's protocol (Qiagen RNA extraction kit and AB high fidelity cDNA synthesis kit), followed by ultraviolet–visible quantification. The detection of each target was achieved by PCR, agarose electrophoresis and SYBR Green Q-PCR detection method with specific primers listed in the Supplementary Information (Supplementary Tables 18 and 19). All gels were detected with Bio-Rad Universal II Molecular Imager and processed with ImageJ (v.1.52p) for any quantitative analysis.

Liquid chromatography and mass spectrometry analysis

Samples were analysed via ultra-performance LC-MS/MS (UPLC-MS/MS). For each time point, 500 µl of mice serum was collected and underwent standard liquid extrusion before LC-MS/MS analysis (see details in Supporting Information). Analysis was performed on a Waters ACQUITY UPLC-I-Class System aligned with a Waters Xevo–TQ-S mass spectrometer (Waters). Liquid chromatographic separation was performed on an Acquity UPLC Charged Surface Hybrid C18 (50 mm × 2.1 mm, 1.7 µm particle size) column at 50 °C. The mobile phase consisted of aqueous 0.1% formic acid, 10 mM ammonium formate solution (mobile phase A) and acetonitrile containing 10 mM ammonium formate in a 0.1% formic acid solution (95:5 *v*/*v*) (mobile phase B). The mass spectrometer was operated in the multiple reaction monitoring mode. Sample introduction and ionization was done by electrospray ionization in the positive and negative ionization mode. MassLynx 4.1 software was used for data acquisition and analysis. The drug concentration for each sample was calculated from a standard linear curve generated by standard sample and internal standard. The mobile phase had a continuous flow rate of 0.60 ml min^{-1} using a time and solvent gradient composition. The detailed analytical procedure and internal standard preparation for each compound can be found in the Supporting Information.

Clinical trial design and data analysis

Institutional review board approval from Partners Healthcare was obtained before any work. Using the Partners RPDR, we retrospectively identified patients on warfarin, tacrolimus, digoxin and levetiracetam therapy who received a short course of doxycycline therapy for an acute infection. All patients were treated at Massachusetts General Hospital or Brigham and Women's Hospital between January 2010 and December 2019. For patients on warfarin therapy, PT-INR values were recorded for the following time periods: 3 months before doxycycline therapy to establish a stable baseline, during doxycycline therapy, 3 days post-doxycycline therapy and 3 months post-doxycycline therapy. For patients on tacrolimus therapy, serum tacrolimus trough levels were recorded for the following time periods: 3 months before doxycycline therapy to establish a stable baseline, during doxycycline therapy, 1 day post-doxycycline therapy and 3 months post-doxycycline therapy. For patients on digoxin therapy, serum digoxin levels were recorded for the following periods: 1 year before doxycycline therapy to establish a stable baseline, during doxycycline therapy, 1 day post-doxycycline therapy and 1 year post-doxycycline therapy. Lastly, for patients on levetiracetam therapy, serum levetiracetam levels were recorded for the following periods: 1 year before doxycycline therapy to establish a stable baseline, during doxycycline therapy, 1 day post-doxycycline therapy and 1 year post-doxycycline therapy. The mean values for these cohorts were calculated and compared using a paired *T*-test between cohorts.

Reporting summary

Further information on research design is available in the Nature Portfolio Reporting Summary linked to this article.

Data availability

The raw and analysed datasets generated during the study are available for research purposes from the corresponding author on reasonable request.

Code availability

All training data and code used for machine learning and to make predictions are available on GitHub at https://github.com/RekerLab/Transportome.

References

1. DeGorter, M. K., Xia, C. Q., Yang, J. J. & Kim, R. B. Drug transporters in drug efficacy and toxicity. *Annu. Rev. Pharmacol. Toxicol.* **52**, 249–273 (2012).
2. Nigam, S. K. What do drug transporters really do? *Nat. Rev. Drug Discov.* **14**, 29–44 (2015).
3. Shitara, Y., Horie, T. & Sugiyama, Y. Transporters as a determinant of drug clearance and tissue distribution. *Eur. J. Pharm. Sci.* **27**, 425–446 (2006).
4. Huang, Y. et al. Membrane transporters and channels: role of the transportome in cancer chemosensitivity and chemoresistance. *Cancer Res.* **64**, 4294–4301 (2004).
5. Brouwer, K. L. et al. In vitro methods to support transporter evaluation in drug discovery and development. *Clin. Pharmacol. Ther.* **94**, 95–112 (2013).

6. Fekete, Z. et al. Membrane assays to characterize interaction of drugs with ABCB1. *J. Membr. Biol.* **248**, 967–977 (2015).
7. International Transporter, C. et al. Membrane transporters in drug development. *Nat. Rev. Drug Discov.* **9**, 215–236 (2010).
8. Pratt, J. et al. Use of zinc finger nuclease technology to knock out efflux transporters in C2BBe1 cells. *Curr. Protoc. Toxicol.* **23**, Unit 23.2 (2012).
9. Sampson, K. E. et al. Zinc finger nuclease-mediated gene knockout results in loss of transport activity for P-glycoprotein, BCRP, and MRP2 in Caco-2 cells. *Drug Metab. Dispos.* **43**, 199–207 (2015).
10. Balimane, P. V. & Chong, S. Cell culture-based models for intestinal permeability: a critique. *Drug Discov. Today* **10**, 335–343 (2005).
11. Ingels, F. M. & Augustijns, P. F. Biological, pharmaceutical, and analytical considerations with respect to the transport media used in the absorption screening system, Caco-2. *J. Pharm. Sci.* **92**, 1545–1558 (2003).
12. Fagerholm, U. Prediction of human pharmacokinetics—gastrointestinal absorption. *J. Pharm. Pharmacol.* **59**, 905–916 (2007).
13. Sun, D. et al. Comparison of human duodenum and Caco-2 gene expression profiles for 12,000 gene sequences tags and correlation with permeability of 26 drugs. *Pharm. Res.* **19**, 1400–1416 (2002).
14. Teksin, Z. S., Seo, P. R. & Polli, J. E. Comparison of drug permeabilities and BCS classification: three lipid-component PAMPA system method versus Caco-2 monolayers. *AAPS J.* **12**, 238–241 (2010).
15. Musther, H., Olivares-Morales, A., Hatley, O. J., Liu, B. & Rostami Hodjegan, A. Animal versus human oral drug bioavailability: do they correlate? *Eur. J. Pharm. Sci.* **57**, 280–291 (2014).
16. Kim, Y. & Chen, J. Molecular structure of human P-glycoprotein in the ATP-bound, outward-facing conformation. *Science* **359**, 915–919 (2018).
17. Aniceto, N., Freitas, A. A., Bender, A. & Ghafourian, T. Simultaneous prediction of four ATP-binding cassette transporters' substrates using multi-label QSAR. *Mol. Inform.* **35**, 514–528 (2016).
18. Sedykh, A. et al. Human intestinal transporter database: QSAR modeling and virtual profiling of drug uptake, efflux and interactions. *Pharm. Res.* **30**, 996–1007 (2013).
19. Karlgren, M. et al. In vitro and in silico strategies to identify OATP1B1 inhibitors and predict clinical drug–drug interactions. *Pharm. Res.* **29**, 411–426 (2012).
20. Jain, S. & Ecker, G. F. In silico approaches to predict drug–transporter interaction profiles: data mining, model generation, and link to cholestasis. *Methods Mol. Biol.* **1981**, 383–396 (2019).
21. Bhhatarai, B., Walters, W. P., Hop, C., Lanza, G. & Ekins, S. Opportunities and challenges using artificial intelligence in ADME/Tox. *Nat. Mater.* **18**, 418–422 (2019).
22. Reker, D. Practical considerations for active machine learning in drug discovery. *Drug Discov. Today Technol.* **32–33**, 73–79 (2019).
23. Montanari, F. & Ecker, G. F. Prediction of drug–ABC-transporter interaction—recent advances and future challenges. *Adv. Drug Deliv. Rev.* **86**, 17–26 (2015).
24. Clerbaux, L. A. et al. Capturing the applicability of in vitro–in silico membrane transporter data in chemical risk assessment and biomedical research. *Sci. Total Environ.* **645**, 97–108 (2018).
25. Gonzalez, L. M., Moeser, A. J. & Blikslager, A. T. Porcine models of digestive disease: the future of large animal translational research. *Transl. Res* **166**, 12–27 (2015).
26. Henze, L. J. et al. The pig as a preclinical model for predicting oral bioavailability and in vivo performance of pharmaceutical oral dosage forms: a PEARRL review. *J. Pharm. Pharmacol.* **1**, 581–602 (2018).
27. Singh, V. K., Thrall, K. D. & Hauer-Jensen, M. Minipigs as models in drug discovery. *Expert Opin. Drug Discov.* **11**, 1131–1134 (2016).
28. von Erlach, T. et al. Robotically handled whole-tissue culture system for the screening of oral drug formulations. *Nat. Biomed. Eng.* **4**, 544–559 (2020).
29. Pietzonka, P., Walter, E., Duda-Johner, S., Langguth, P. & Merkle, H. P. Compromised integrity of excised porcine intestinal epithelium obtained from the abattoir affects the outcome of in vitro particle uptake studies. *Eur. J. Pharm. Sci.* **15**, 39–47 (2002).
30. Neirinckx, E. et al. Feasibility of the Ussing chamber technique for the determination of in vitro jejunal permeability of passively absorbed compounds in different animal species. *J. Vet. Pharm. Ther.* **34**, 290–297 (2011).
31. Westerhout, J. et al. A new approach to predict human intestinal absorption using porcine intestinal tissue and biorelevant matrices. *Eur. J. Pharm. Sci.* **63**, 167–177 (2014).
32. Gerber, W., Hamman, J. H. & Steyn, J. D. Excipient–drug pharmacokinetic interactions: effect of disintegrants on efflux across excised pig intestinal tissues. *J. Food Drug Anal.* **26**, S115–S124 (2018).
33. Arnold, Y. E. & Kalia, Y. N. Using ex vivo porcine jejunum to identify membrane transporter substrates: a screening tool for early-stage drug development. *Biomedicines* **8**, 340 (2020).
34. Arnold, Y. E., Thorens, J., Bernard, S. & Kalia, Y. N. Drug transport across porcine intestine using an Ussing chamber system: regional differences and the effect of P-glycoprotein and CYP3A4 activity on drug absorption. *Pharmaceutics* **11**, 139 (2019).
35. Wishart, D. S. et al. DrugBank 5.0: a major update to the DrugBank database for 2018. *Nucleic Acids Res.* **46**, D1074–D1082 (2018).
36. Haimeur, A., Conseil, G., Deeley, R. G. & Cole, S. P. The MRP-related and BCRP/ABCG2 multidrug resistance proteins: biology, substrate specificity and regulation. *Curr. Drug Metab.* **5**, 21–53 (2004).
37. Johnson, Z. L. & Chen, J. Structural basis of substrate recognition by the multidrug resistance protein MRP1. *Cell* **168**, 1075–1085 e1079 (2017).
38. Englund, G. et al. Regional levels of drug transporters along the human intestinal tract: co-expression of ABC and SLC transporters and comparison with Caco-2 cells. *Eur. J. Pharm. Sci.* **29**, 269–277 (2006).
39. Kunta, J. R. & Sinko, P. J. Intestinal drug transporters: in vivo function and clinical importance. *Curr. Drug Metab.* **5**, 109–124 (2004).
40. Estudante, M., Morais, J. G., Soveral, G. & Benet, L. Z. Intestinal drug transporters: an overview. *Adv. Drug Deliv. Rev.* **65**, 1340–1356 (2013).
41. Van Peer, E. et al. Ontogeny of CYP3A and P-glycoprotein in the liver and the small intestine of the Gottingen minipig: an immunohistochemical evaluation. *Basic Clin. Pharmacol. Toxicol.* **114**, 387–394 (2014).
42. Tang, H., Pak, Y. & Mayersohn, M. Protein expression pattern of P-glycoprotein along the gastrointestinal tract of the Yucatan micropig. *J. Biochem. Mol. Toxicol.* **18**, 18–22 (2004).
43. Mouly, S. & Paine, M. F. P-glycoprotein increases from proximal to distal regions of human small intestine. *Pharm. Res.* **20**, 1595–1599 (2003).
44. Tang, H. & Mayersohn, M. Porcine prediction of pharmacokinetic parameters in people: a pig in a poke?*Drug Metab. Dispos.* **46**, 1712–1724 (2018).
45. Schoellhammer, C. M. et al. Ultrasound-mediated delivery of RNA to colonic mucosa of live mice. *Gastroenterology* **152**, 1151–1160 (2017).
46. Schoellhammer, C. M. & Traverso, G. Low-frequency ultrasound for drug delivery in the gastrointestinal tract. *Expert Opin. Drug Deliv.* **13**, 1045–1048 (2016).
47. Konig, J., Muller, F. & Fromm, M. F. Transporters and drug–drug interactions: important determinants of drug disposition and effects. *Pharm. Rev.* **65**, 944–966 (2013).

48. FDA. *Drug Development and Drug Interactions* (US Food and Drug, 2019); https://www.fda.gov/Drugs/DevelopmentApprovalProcess/DevelopmentResources/DrugInteractionsLabeling/ucm093664.htm
49. Shugarts, S. & Benet, L. Z. The role of transporters in the pharmacokinetics of orally administered drugs. *Pharm. Res.* **26**, 2039–2054 (2009).
50. Mak, L. et al. Metrabase: a cheminformatics and bioinformatics database for small molecule transporter data analysis and (Q)SAR modeling. *J. Cheminform* **7**, 31 (2015).
51. Szakacs, G. et al. Predicting drug sensitivity and resistance: profiling ABC transporter genes in cancer cells. *Cancer Cell* **6**, 129–137 (2004).
52. Wallqvist, A., Rabow, A. A., Shoemaker, R. H., Sausville, E. A. & Covell, D. G. Linking the growth inhibition response from the National Cancer Institute's anticancer screen to gene expression levels and other molecular target data. *Bioinformatics* **19**, 2212–2224 (2003).
53. Reker, D., Schneider, P., Schneider, G. & Brown, J. B. Active learning for computational chemogenomics. *Future Med. Chem.* **9**, 381–402 (2017).
54. Reker, D., Schneider, P. & Schneider, G. Multi-objective active machine learning rapidly improves structure–activity models and reveals new protein–protein interaction inhibitors. *Chem. Sci.* **7**, 3919–3927 (2016).
55. Amin, M. L. P-glycoprotein inhibition for optimal drug delivery. *Drug Target Insights* **7**, 27–34 (2013).
56. Lemos, C., Jansen, G. & Peters, G. J. Drug transporters: recent advances concerning BCRP and tyrosine kinase inhibitors. *Br. J. Cancer* **98**, 857–862 (2008).
57. Houghton, P. J. et al. Imatinib mesylate is a potent inhibitor of the ABCG2 (BCRP) transporter and reverses resistance to topotecan and SN-38 in vitro. *Cancer Res.* **64**, 2333–2337 (2004).
58. Horikawa, M., Kato, Y., Tyson, C. A. & Sugiyama, Y. The potential for an interaction between MRP2 (ABCC2) and various therapeutic agents: probenecid as a candidate inhibitor of the biliary excretion of irinotecan metabolites. *Drug Metab. Pharmacokinet.* **17**, 23–33 (2002).
59. Kim, K. A., Oh, S. O., Park, P. W. & Park, J. Y. Effect of probenecid on the pharmacokinetics of carbamazepine in healthy subjects. *Eur. J. Clin. Pharm.* **61**, 275–280 (2005).
60. Gupta, A. et al. Cyclosporin A, tacrolimus and sirolimus are potent inhibitors of the human breast cancer resistance protein (ABCG2) and reverse resistance to mitoxantrone and topotecan. *Cancer Chemother. Pharmacol.* **58**, 374–383 (2006).
61. Poller, B., Wagenaar, E., Tang, S. C. & Schinkel, A. H. Double-transduced MDCKII cells to study human P-glycoprotein (ABCB1) and breast cancer resistance protein (ABCG2) interplay in drug transport across the blood–brain barrier. *Mol. Pharm.* **8**, 571–582 (2011).
62. Lai, Y. et al. Preclinical and clinical evidence for the collaborative transport and renal secretion of an oxazolidinone antibiotic by organic anion transporter 3 (OAT3/SLC22A8) and multidrug and toxin extrusion protein 1 (MATE1/SLC47A1). *J. Pharmacol. Exp. Ther.* **334**, 936–944 (2010).
63. Mu, J. et al. Multiple transporters associated with malaria parasite responses to chloroquine and quinine. *Mol. Microbiol.* **49**, 977–989 (2003).
64. Endres, C. J., Hsiao, P., Chung, F. S. & Unadkat, J. D. The role of transporters in drug interactions. *Eur. J. Pharm. Sci.* **27**, 501–517 (2006).
65. Noe, J., Portmann, R., Brun, M. E. & Funk, C. Substrate-dependent drug–drug interactions between gemfibrozil, fluvastatin and other organic anion-transporting peptide (OATP) substrates on OATP1B1, OATP2B1, and OATP1B3. *Drug Metab. Dispos.* **35**, 1308–1314 (2007).
66. Ichihara, S. et al. Association of a polymorphism of ABCB1 with obesity in Japanese individuals. *Genomics* **91**, 512–516 (2008).

Acknowledgements

D.R. is a Swiss National Science Foundation Fellow (grant P2EZP3_168827 and P300P2_177833). This work was in part supported by NIH grant EB000244 (G.T., R.L.), the Karl van Tassel (1925) Career Development Professorship and Department of Mechanical Engineering MIT and Division of Gastroenterology, Brigham and Women's Hospital (G.T.). The clinical work was in part supported by a Prostate Cancer Foundation Young Investigator Award (J.D.B.). Z.F. is supported by the Department of Defense through the National Defense Science and Engineering Graduate Fellowship Program. Z.Z. is supported by a Fellowship from the Department of Biomedical Engineering at Duke University. The authors acknowledge the use of resources of Microscopy Core Facilities at Swanson Biotechnology Center, David H. Koch Institute for Integrative Cancer Research at MIT, and G. Church for sharing the cell line PK15. The authors also acknowledge Partners RPDR team for their assistance with identifying patients and M. Jimenez for his substantial contributions to editing the manuscript.

Author contributions

Y.S., D.R., J.D.B., A.R.K. and G.T. conceived the study, designed experiments and analysed data. K.H., Z.W., N.N., Z.F., Z.Z., A.L., V.S., J.W., T.v.E., C.C.Y. and L.M. performed experiments and analysed data. Y.S., D.R., J.D.B., A.R.K. and G.T. wrote the manuscript. R.L. and G.T. supervised the study. All authors discussed the results and assisted in the preparation of the manuscript.

Competing interests

Y.S., D.R., V.S., R.L. and G.T. are co-inventors on a provisional patent application encompassing the work described. T.v.E., R.L. and G.T. have a financial interest in Vivtex, a biotechnology company applying ex vivo models for high-throughput drug formulation development. D.R. acts as a consultant to the pharmaceutical and biotechnology industry. Complete details of all relationships for profit and not for profit for G.T. and for R.L. can be found in the Supplementary Information.

Additional information

Extended data is available for this paper at https://doi.org/10.1038/s41551-023-01128-9.

Supplementary information The online version contains supplementary material available at https://doi.org/10.1038/s41551-023-01128-9.

Correspondence and requests for materials should be addressed to Giovanni Traverso.

Peer review information *Nature Biomedical Engineering* thanks Alexander Tropsha and the other, anonymous, reviewer(s) for their contribution to the peer review of this work.

https://doi.org/10.1038/s41551-023-01128-9

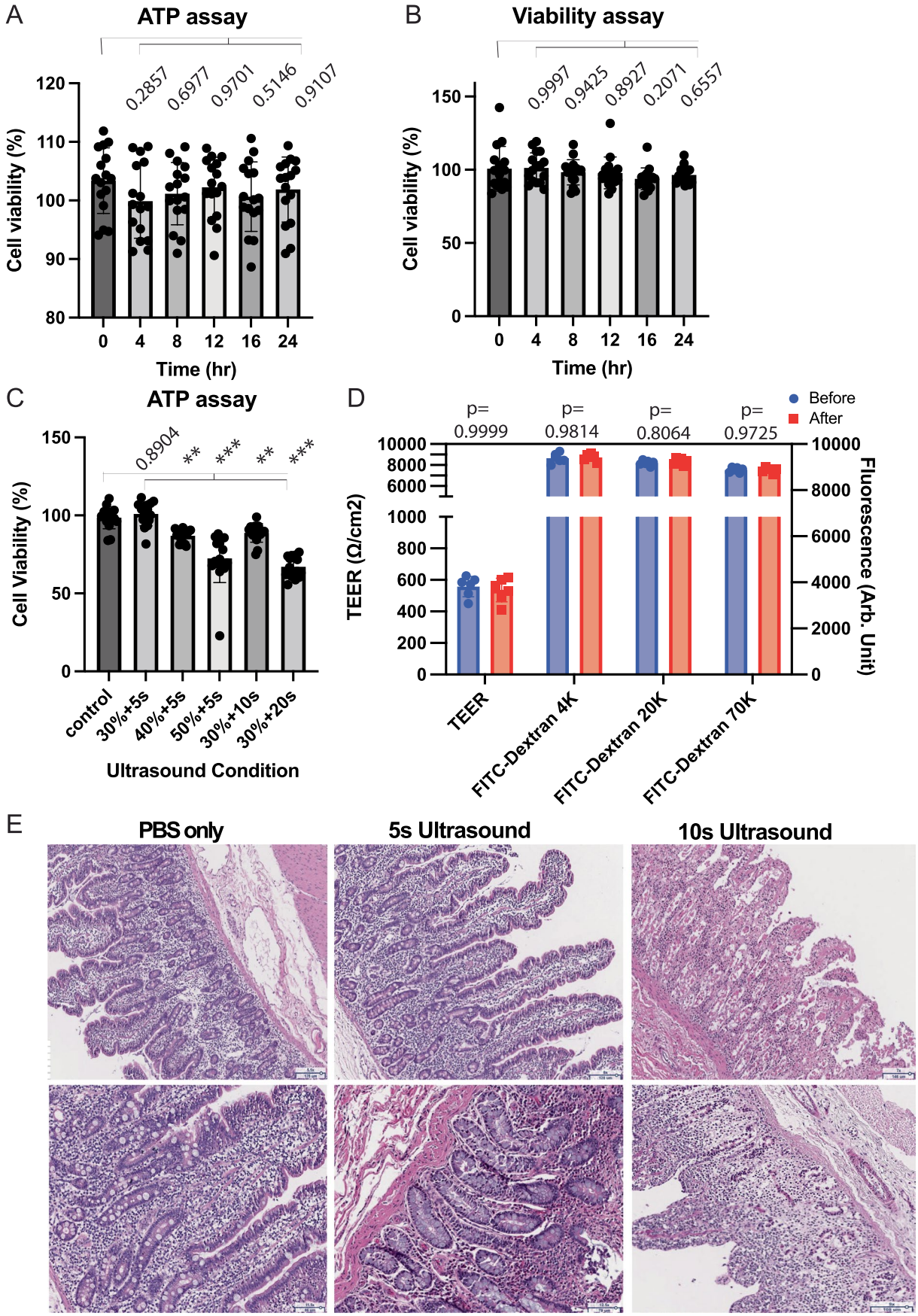

Extended Data Fig. 1 | See next page for caption.

https://doi.org/10.1038/s41551-023-01128-9

Extended Data Fig. 1 | Tissue viability assay and H&E histology staining to assess the safety and toxicity effect of *ex vivo culture* and low-frequency ultrasound on pig small intestine. ATP and CellTiter-Glo assay were performed on ex vivo tissue cultured tissue with different time points to monitor the metabolic activity (**a**) and viability (**b**) of sliced tissue. **c**) ATP assay on ex vivo tissue at different ultrasound conditions to monitor damage caused by ultrasound delivery. **d**) TEER and FITC-labeled Dextran permeability assays to evaluate the possibility for changes in tissue permeability in response to low-frequency ultrasound treatment. In all experiments, three separate animal tissues were included and four repeats were performed for each tissue (n = 12). **e**) H&E histology staining using fresh tissue, tissue after a short ultrasound treatment, and tissue after a prolonged ultrasound treatment.

https://doi.org/10.1038/s41551-023-01128-9

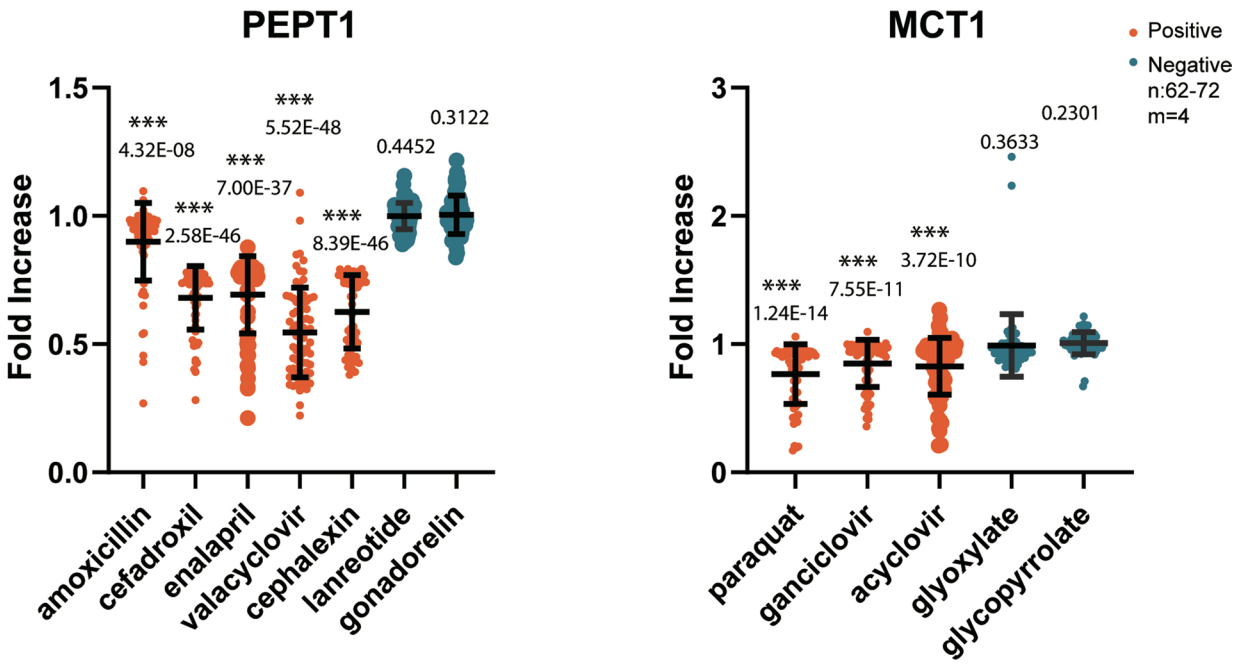

Extended Data Fig. 2 | Validation of the *ex vivo* system for fold decrease of substrates/non-substrates of PEPT1 (A) and MCT1 (B) through the siRNA-mediated knock down of drug transporters of GI-TRIS. Perfusion decreases for substrates because these enzymes are influx transporters.

https://doi.org/10.1038/s41551-023-01128-9

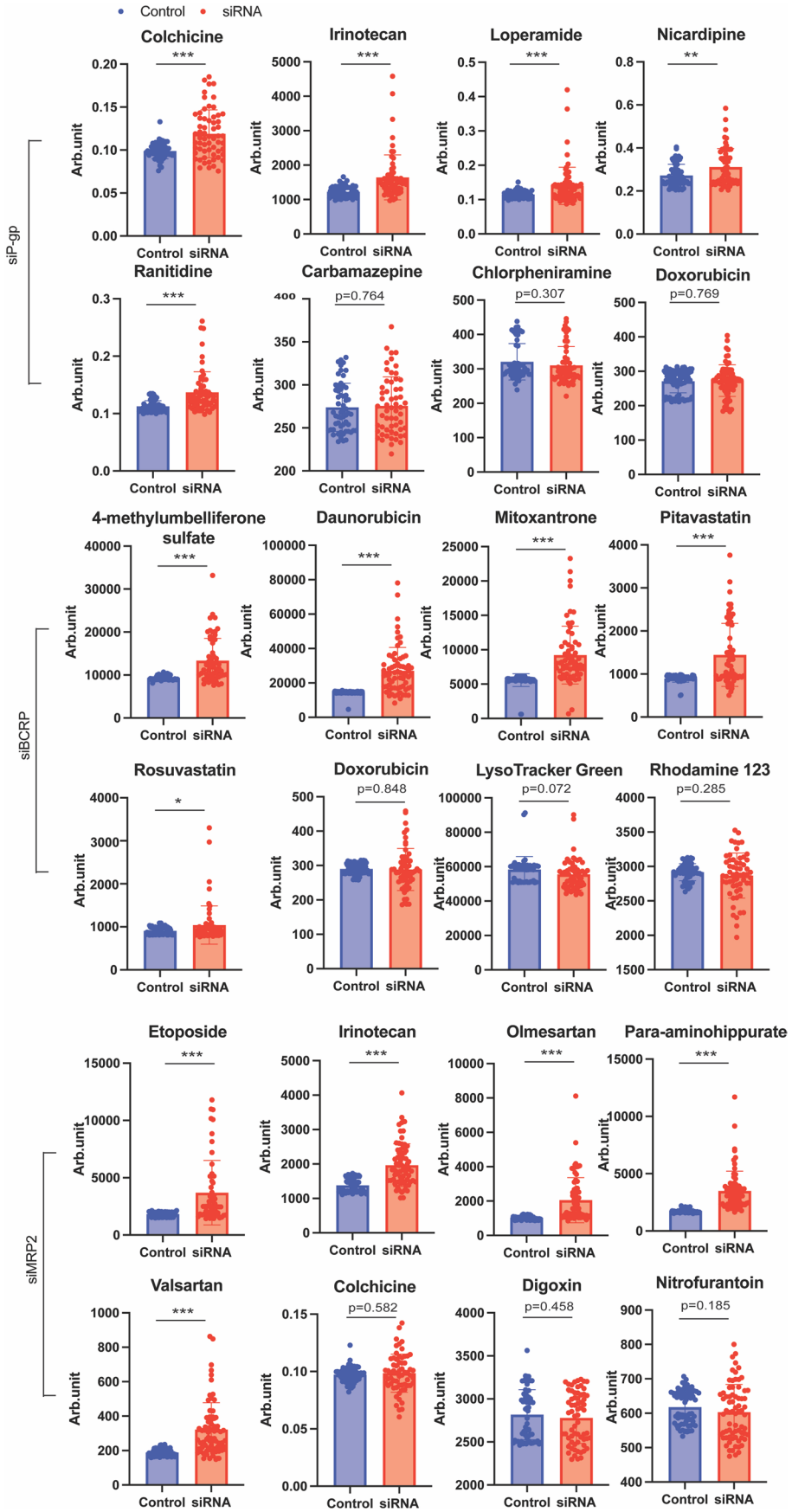

Extended Data Fig. 3 | See next page for caption.

https://doi.org/10.1038/s41551-023-01128-9

Extended Data Fig. 3 | Original data for substrate perfusion with siRNA treatment in the *ex vivo* system. For each drug, the data is collected from 62–72 trials (n = 62–72) of tissue in four different pigs (m = 4). For siP-gp treated samples, Colchicine, Irinotecan, Loperamide, Nicardipine and Ranitidine are drug transporter specific substrates, while Carbamazepine, Chlorpheniramine, and Doxorubicin are non-specific substrates. For siBCRP treated samples, 4-methylumbelliferone sulfate, Daunorubicin, Mitoxantrone, Pitavastatin, and Rosuvastatin are BCRP specific substrates, while Doxorubicin, LysoTracker Green, and Rhodamine 123 are non-specific substrates. For siMRP2 treated samples, Etoposide, Irinotecan, Olmesartan, Para-aminohippurate, and Valsartan are MRP2 specific substrates, while Colchicine, Digoxin, and Nitrofurantoin are non-specific substrates.

nature portfolio

Corresponding author(s): Giovanni Traverso

Last updated by author(s): Jan 18, 2024

Reporting Summary

Nature Portfolio wishes to improve the reproducibility of the work that we publish. This form provides structure for consistency and transparency in reporting. For further information on Nature Portfolio policies, see our Editorial Policies and the Editorial Policy Checklist.

Statistics

For all statistical analyses, confirm that the following items are present in the figure legend, table legend, main text, or Methods section.

n/a	Confirmed
☐	☒ The exact sample size (*n*) for each experimental group/condition, given as a discrete number and unit of measurement
☐	☒ A statement on whether measurements were taken from distinct samples or whether the same sample was measured repeatedly
☐	☒ The statistical test(s) used AND whether they are one- or two-sided *Only common tests should be described solely by name; describe more complex techniques in the Methods section.*
☐	☒ A description of all covariates tested
☐	☒ A description of any assumptions or corrections, such as tests of normality and adjustment for multiple comparisons
☐	☒ A full description of the statistical parameters including central tendency (e.g. means) or other basic estimates (e.g. regression coefficient) AND variation (e.g. standard deviation) or associated estimates of uncertainty (e.g. confidence intervals)
☐	☒ For null hypothesis testing, the test statistic (e.g. *F*, *t*, *r*) with confidence intervals, effect sizes, degrees of freedom and *P* value noted *Give P values as exact values whenever suitable.*
☒	☐ For Bayesian analysis, information on the choice of priors and Markov chain Monte Carlo settings
☒	☐ For hierarchical and complex designs, identification of the appropriate level for tests and full reporting of outcomes
☒	☐ Estimates of effect sizes (e.g. Cohen's *d*, Pearson's *r*), indicating how they were calculated

Our web collection on statistics for biologists contains articles on many of the points above.

Software and code

Policy information about availability of computer code

Data collection	We collected data from DrugBank (5.0), Metrabase (v 1.0) and the NIH NCI-60 dataset. Data were processed with a custom data-science workflow implemented in KNIME (version 4.1.2) and fully described in Methods. All data are available from GitHub at https://github.com/RekerLab/Transportome.
Data analysis	Data were analysed using Prism (version 7) and using Python (2.6). Machine learning was performed in scikit-learn and DeepChem, and all code to perform model training and evaluation is available from GitHub at https://github.com/RekerLab/Transportome.

For manuscripts utilizing custom algorithms or software that are central to the research but not yet described in published literature, software must be made available to editors and reviewers. We strongly encourage code deposition in a community repository (e.g. GitHub). See the Nature Portfolio guidelines for submitting code & software for further information.

Data

Policy information about availability of data

All manuscripts must include a data availability statement. This statement should provide the following information, where applicable:

- Accession codes, unique identifiers, or web links for publicly available datasets
- A description of any restrictions on data availability
- For clinical datasets or third party data, please ensure that the statement adheres to our policy

The raw and analysed datasets generated during the study are available for research purposes from the corresponding author on reasonable request.

Human research participants

Policy information about studies involving human research participants and Sex and Gender in Research.

Reporting on sex and gender	Sex and gender were not identified in the retrospective analyses.
Population characteristics	We retrospectively identified patients on warfarin, tacrolimus, digoxin and levetiracetam therapy who received a short course of doxycycline therapy for an acute infection. All patients were treated at Massachusetts General Hospital or Brigham and Women's Hospital between January 2010 and December 2019.
Recruitment	Patients were retrospectively identified through the Partners Research Patient Data Registry. Informed consent was waived owing to the retrospective nature of the studies.
Ethics oversight	IRB exempt by Partners Healthcare (protocol #2019P003506).

Note that full information on the approval of the study protocol must also be provided in the manuscript.

Field-specific reporting

Please select the one below that is the best fit for your research. If you are not sure, read the appropriate sections before making your selection.

☒ Life sciences ☐ Behavioural & social sciences ☐ Ecological, evolutionary & environmental sciences

For a reference copy of the document with all sections, see nature.com/documents/nr-reporting-summary-flat.pdf

Life sciences study design

All studies must disclose on these points even when the disclosure is negative.

Sample size	For experiments involving the ex vivo validation of interactions between drug transporters and known inhibitors, a total of 62–74 replicates from 4 distinct pig tissues were chosen on the basis of minimal requirements for obtaining meaningful statistical results. For the ex vivo screening of drug-transporter interactions with 28 commercial drugs, a total of 12 replicates from 4 different animals are included. This decision was based on minimal requirements for obtaining meaningful statistical results. For the in vivo mice experiments of drug–drug interactions via targeting the same drug transporter, the n = 5 for each time point was decided according to the current standard for pharmacokinetics in mice. For the in vivo clinical data, each condition contains a range of 43–50 patients. This number was decided on the basis of both the standard in achieving a statistically significant result and the size of the clinical database.
Data exclusions	For replicates, when leakage was observed on plates or wells, the corresponded data points were excluded. Otherwise, all data were included in the analysis.
Replication	Each experiment was repeated in multiple animals with various number of replicates (between 3 to 5 animals per experiment). The number of animals and replicates are all indicated in the text.
Randomization	The animals were assigned randomly to experimental and control groups.
Blinding	The design, execution and data analyses of this study were performed by different individuals to make sure that they were blinded to the data.

Reporting for specific materials, systems and methods

We require information from authors about some types of materials, experimental systems and methods used in many studies. Here, indicate whether each material, system or method listed is relevant to your study. If you are not sure if a list item applies to your research, read the appropriate section before selecting a response.

Materials & experimental systems

n/a	Involved in the study
☐	☒ Antibodies
☐	☒ Eukaryotic cell lines
☒	☐ Palaeontology and archaeology
☐	☒ Animals and other organisms
☐	☒ Clinical data
☒	☐ Dual use research of concern

Methods

n/a	Involved in the study
☒	☐ ChIP-seq
☒	☐ Flow cytometry
☒	☐ MRI-based neuroimaging

Antibodies

Antibodies used

P-gp LSBio (aa863-912) 1:250 Rb
BCRP abcam (ab63907) 1:1000 Rb
MRP2 abcam (ab110740) 1:500 Rb
MCT1 abcam(ab90582) 1:500 Rb
SNAT2 abcam (ab90677) 1:1000 Rb
OST-a abcam (ab103442) 1:500 Rb
PEPT1 santa curze (sc-373742) 1:1000 Ms
OCT1 abcam (ab180749) 1:500 Rb
ABCC3 sigma aldrich (SAB2100011); LSBio (LS-C829592); abcam (ab232971) 1:250-1:1000 Rb
GAPDH abcam (ab9484) 1:2000 Ms
Actin abcam (ab8227) 1:2000 Rb
anti-mouse (HRP) abcam (ab6728) 1:3000 Rb
anti-rabbit (HRP) abcam (ab6721) 1:1000 Gt

Validation

Product anti-BCRP(abcam: ab63907) has been stated by the Abcam website to react with pig BCRP r protein for western blotting application. Product anti-GAPDH (abcam: ab9484) was validated by Abcam to react with pig liver tissue with western blot. Product anti-PEPT1 (santa curze, sc-373742) was reported on Santa curze website for detection of porcine intestinal PEPT1 with WB. Product anti-MRP3 (abcam, ab232971) was validated by ABcam for reacting with pig liver lysate detected by WB.

Eukaryotic cell lines

Policy information about cell lines and Sex and Gender in Research

Cell line source(s)	PK15 (pig), gifted by George Church.
Authentication	None of the cell lines were authenticated.
Mycoplasma contamination	The cell lines were not tested for mycoplasma contamination, but no indication of contamination was observed.
Commonly misidentified lines (See ICLAC register)	No commonly misidentified cell lines were used.

Animals and other research organisms

Policy information about studies involving animals; ARRIVE guidelines recommended for reporting animal research, and Sex and Gender in Research

Laboratory animals	10–12-weeks-old female Balb/c mice from Charles River and The Jackson Laboratory.
Wild animals	The study did not involve wild animals.
Reporting on sex	Female mice. Porcine tissues were of mixed gender.
Field-collected samples	The study did not involve samples collected from the field.
Ethics oversight	All animal procedures were conducted in accordance with protocols approved by the Massachusetts Institute of Technology Committee on Animal Care.

Note that full information on the approval of the study protocol must also be provided in the manuscript.

Clinical data

Policy information about clinical studies

All manuscripts should comply with the ICMJE guidelines for publication of clinical research and a completed CONSORT checklist must be included with all submissions.

Clinical trial registration	We carried out a retrospective study. Institutional Review Board (IRB) approval from Partners Healthcare was obtained prior to any work.
Study protocol	See 'Clinical trial design and data analysis' in Methods.
Data collection	We retrospectively identified patients on warfarin, tacrolimus, digoxin and levetiracetam therapy who received a short course of doxycycline therapy for an acute infection. All patients were treated at Massachusetts General Hospital or Brigham and Women's Hospital between January 2010 and December 2019.
Outcomes	We found a significant increase of all four tested drugs when co-administrated with doxycycline, with the levels returning to baseline after completion of doxycycline therapy. More information and context is provided in Results.